Hindawi
Journal of Chemistry
Volume 2020, Article ID 8456194, 8 pages
https://doi.org/10.1155/2020/8456194

Research Article

Synthesis and Characterization of Mesoporous Silica SBA-15 and ZnO/SBA-15 Photocatalytic Materials from the Ash of Brickyards

Quach Nguyen Khanh Nguyen,[1] Nguyen Thi Yen,[1] Nguyen Duc Hau,[1] and Hoai Lam Tran [2]

[1]*Saigon University, Ho Chi Minh City 700000, Vietnam*
[2]*Ho Chi Minh City University of Food Industry, Ho Chi Minh City 700000, Vietnam*

Correspondence should be addressed to Hoai Lam Tran; hoailamud@gmail.com

Received 19 October 2019; Accepted 17 February 2020; Published 19 March 2020

Guest Editor: Yin-Ting Yeh

SBA-15 has been successfully synthesized from ash of brickyard with the surface area of 700.100 m^2/g, pore volume of 0.813 $cm^3 \cdot g^{-1}$, and pore size of 7.5 nm. SBA-15 material has been modified by a simple impregnation method, and the ZnO/SBA-15 obtained material retains the hexagonal structure of SBA-15, but the hexagonal capillary tube size is reduced, in which the surface area, volume of pores, and pore size is 212.851 $m^2 \cdot g^{-1}$, 0.244 $cm^3 \cdot g^{-1}$, and 3.7 nm, respectively. The ZnO/SBA-15 materials were investigated by the photodegradation of methylene blue under ultraviolet light and exhibited significant photocatalytic activity with the reached MB removal efficiency about 96.69%.

1. Introduction

SBA-15 is a mesoporous silica sieve based on uniform hexagonal pores with a narrow pore size distribution and a tunable pore diameter of between 5 and 15 nm [1]. The important properties of SBA-15 such as high surface area of typically 400–900 $m^2 \cdot g^{-1}$, high thermal and mechanical stability, inert, and not harmful to the environment make SBA-15 a well-suited material for various applications. It can be used in environmental treatment for adsorption and separation [2, 3], as a support material for catalysts [4, 5] and as a template for the production of ordered mesoporous carbon [6].

SBA-15 is usually synthesized in a cooperative self-assembly process under acidic conditions using the triblock copolymer pluronic 123 ($EO_{20}PO_{70}EO_{20}$) as template and tetraethoxysilane (TEOS) as the silica source [1–7]. However, high cost of complex TEOS processing motivates the development of alternative silica source. The recent studies are the synthesis of highly siliceous SBA-15 from inorganic silica sources as sodium silicate [8] and the silica inorganic precursor with the presence of impurities of industrial waste product which typically consist of metal oxide containing 42 wt% SiO_2 [9].

In this paper, the ash of brickyards was used as the silica precursor for preparation of mesoporous silica SBA-15 because its main component was the rice husk ash that has high silica content. In Vietnam, the rice husk ash of brickyards is an abundantly available waste material; therefore, SBA-15 synthesized by using rice husk ash as the silica source will bring economic efficiency.

Moreover, the mesoporous silica SBA-15 materials are particularly interesting as host matrices for loading metals and semiconductor nanoparticles. These supported metal oxide particles have important applications in photocatalysis [10, 11]. In this study, to further improve the efficiency of the treatment of dyers, ZnO has been chosen to develop on internal and external surfaces of SBA-15 materials by the impregnation method. Recent studies have demonstrated the good photocatalysis of ZnO in the decomposition reactions of toxic organic compounds in wastewater due to high quantum efficiency, redox potential, high physicochemical stability, nontoxicity, and low cost [12–14].

2. Materials and Methods

2.1. Preparation of SBA-15. The ash of brickyard was cleaned and stirred in concentrated NaOH solution at 100°C for 3 h. Then, the mixture was filtered with activated carbon to obtain a transparent solution (solution A).

SBA-15 was synthesized under strong acidic condition (pH = 1) using the triblock copolymer pluronic 123 ($EO_{20}PO_{70}EO_{20}$) as the template [1] and solution A as the silica source.

2.2. Preparation of ZnO/SBA-15. ZnO/SBA-15 was synthesized by impregnating SBA-15 with zinc acetate solution. 0.901 g Zn $(CH_3COO)_2.2H_2O$ was dissolved in 42 mL of ethanol solvent along with stirring at 70°C for 2 hours. The obtained solution was cooled down to room temperature, and then was added 0.5 g SBA-15 with strong stirring. The resulting mixture was dried at 80°C for 24 hours to remove the solvent. Then, the obtained samples were calcinated in air by raising the temperature from room temperature to 550 oC over 1 hour period and holding at 550 oC for 1 hour

2.3. Structural Characteristics Analysis. FTIR spectra were obtained by using a FTIR-8400S Shimadzu spectrometer. X-Ray diffraction patterns were recorded by the D2 phaser system using Cu Kα radiation ($\lambda = 1.54$ Å) with 2θ of 10° to 80° and by Bruker D8 Advance using Cu Kα radiation ($\lambda = 1.54$ Å) with 2θ of 0.1° to 10°. The nitrogen adsorption/desorption isotherms were surveyed by a Quantachrome Nova 2000e meter, measured isothermal adsorption N_2 at 77 K and the adsorption rate of desorption P/P_o from 0.01–0.99, by taking surface area from 0.05–0.35. The structure of materials is observed via TEM images and recorded on a JEOL apparatus (model: JEM-1400, Japan) with 100 kV voltage. The samples were dispersed in the ethanol solvent and then put on the net with Cu. The sample preparation technique is used for recording scanning electron microscopic images (SEM) and analyzing EDS on the same device. The sample recorded image on JSM–IT200 InTouchScope™ scanning electron microscope.

2.4. Experimental Protocol of Methylene Blue Removal. In this section, the light of the ultraviolet lamp 50 W was chosen to investigate the photocatalytic activities of ZnO/SBA-15 materials because ZnO is appropriate for short wavelength optoelectronics [11–13].

The experiments were carried out in 100 mL Erlenmeyer flask by mixing 25 mg ZnO/SBA-15 adsorbents and 50 mL of MB solution with 56 ppm of initial concentration. The solution was stirred at 600 rpm on a stirrer at a constant temperature for 10 min in the dark to equilibrate and then stirred for 60 min under ultraviolet light. After shaking the solution, the reaction mixtures were centrifuged, and the filtrate was analyzed using a spectrophotometer. The adsorbed quantity and removal efficiency of MB were calculated using equations (1) and (2), respectively:

$$q_e = \frac{(C_o - C_e)V}{m}, \tag{1}$$

$$\%\ \text{removal} = \frac{C_o - C_e}{C_o} \cdot 100, \tag{2}$$

where q_e is the amount of dye in mg per gram of adsorbent. C_o and C_e are, respectively, initial concentration and equilibrium time of MB ($mg{\cdot}L^{-1}$). V is the volume of solution. m is the mass of adsorbent.

2.4.1. Effect of Photocatalytic Time on MB Removal Capability. 5 mg ZnO/SBA-15 was added to 50 mL MB solution with initial concentration, $C_o = 56$ ppm. The mixture was stirred for 10 min in the dark to equilibrate and then stirred for 30 min to 360 min under ultraviolet light.

2.4.2. Effect of Solid/Liquid Ratio on the Adsorption and Photocatalytic Capacity of ZnO/SBA-15. The solid/liquid ratio is determined by the following formula:

$$\sigma = \frac{m_{\text{ZnO/SBA-15}}}{V_{\text{MB}}}, \tag{3}$$

where $m_{\text{ZnO/SBA-15}}$ is the weight of ZnO/SBA-15 and V_{MB} is 50 mL methylene blue solution.

The solid/liquid ratios of 0.1 to 3 were selected to investigate the removal capacity of ZnO/SBA-15. The mixture was stirred for 10 min in the dark and 60 min under ultraviolet light.

3. Results and Discussion

3.1. Structural Characteristics of SBA-15 Materials. SBA-15 synthesized from rice husk ash was analyzed using the FTIR infrared spectrum is shown in Figure 1. In the FTIR pattern, a broad peak at 3500 cm^{-1} is the O-H bond stretching vibration of the silanol groups and the remaining absorbed water molecules in the samples. The presence of a weak peak at 2890 cm^{-1} is supposed to be C-H stretching vibration, and it suggests that almost all surfactant was ousted. The bending vibration of the O-H of water appears at wavenumber 1635 cm^{-1}. The strong characteristic peak of siloxane (-Si-O-Si-) appears at 1082 cm^{-1}. The Si-OH bond stretching vibration of the silanol groups is observed at 961 cm^{-1}, and the Si-O bond rocking vibration was shown at 490 cm^{-1}. These functional groups correspond to the FTIR pattern of SBA-15 from TEOS [1].

XRD pattern of the SBA-15 sample is shown in Figure 2. Figure 2(a) shows the small-angle XRD patterns of SBA-15, scan range of 2 theta degrees of 0.5° to 10°. The typical XRD pattern for SBA-15 exhibits three characteristic peaks relative to the (100), (110), and (200) planes at 2θ of 0.96°, 1.45°, and 1.7°. These peaks characterize the two-dimensional hexagonal structure of SBA-15 which matches SBA-15 synthesized using TEOS as the silica source. So, SBA-15 material was successfully synthesized from the ash of brickyards.

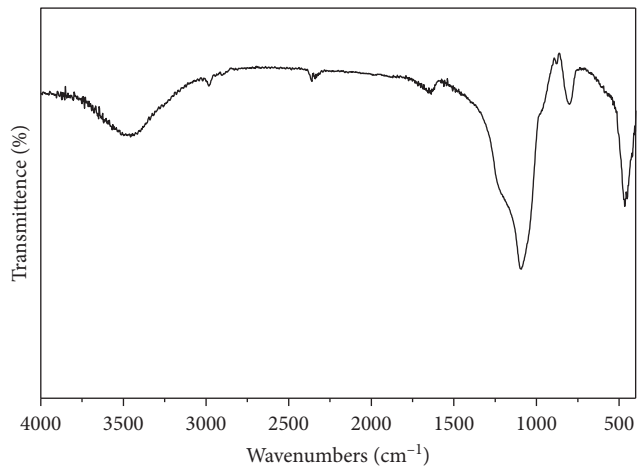

Figure 1: FT-IR spectra of SBA-15.

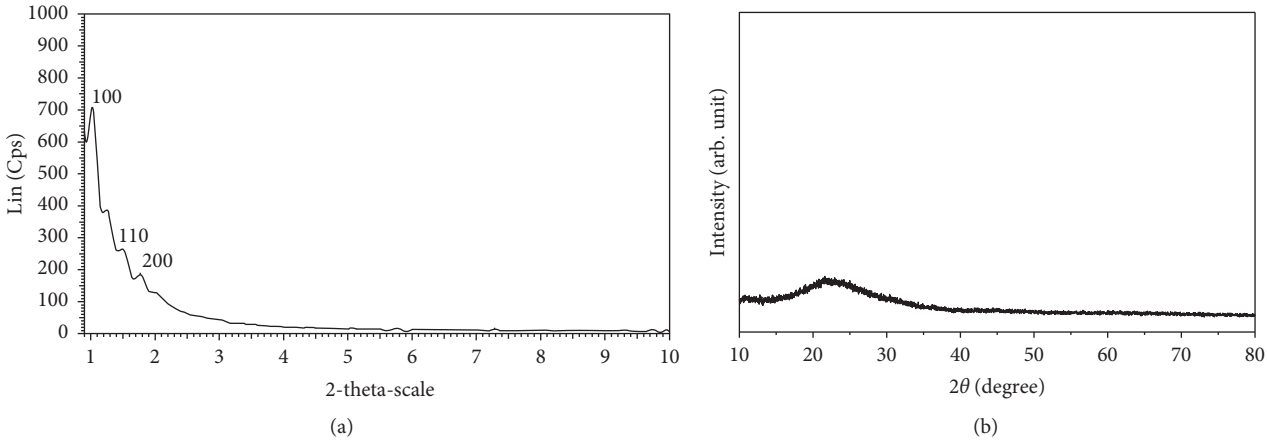

Figure 2: The small-angle XRD pattern (a) and the high-angle XRD pattern (b) of SBA-15.

The high-angle XRD pattern of SBA-15, scan range 2θ of 10°–80° is shown in Figure 2(b) shows that there is no SiO_2 crystal phase in SBA-15, so we can confirm the porous structure of SBA-15 is SiO_2 amorphous.

The porosity and capillary structure of SBA-15 and ZnO/SBA-15 materials were studied by nitrogen adsorption/desorption isotherms and are shown in Figures 3 and 4. IUPAC adsorption isotherm of type IV shows that SBA-15 belongs to mesoporous material with mesopore size. In addition, the hysterics type of H1 is characteristic of mesoporous materials with cylindrical pores and has a uniform pores size. Figure 3(b) shows the SBA-15 synthesized from the ash of brickyards with uniform pore size and concentrated in 6–12 nm.

From the data obtained by the BET method to calculate the surface area of the SBA-15 is 700.10 m^2/g, the volume of pores and pore size, respectively: 0.813 cm^3/g and 7.5 nm. On the contrary, the molecule methylene blue is seen as a rectangular box with dimensions $17.0 \times 7.6 \times 3.3$ A [15]. Therefore, SBA-15 synthesized from the rice husk ash with size suitable for good adsorption of methylene blue.

TEM images of SBA-15 are shown in Figure 5 with the parallel, uniform channels (Figure 5(a)), and hexagonal structure has formed with uniform pore size, about 7.8 nm (Figure 5(b)).

3.2. Structural Characteristics of ZnO/SBA-15 Materials. Figure 6(a) displays the high-angle XRD patterns of ZnO/SBA-15. XRD patterns show the peaks at $2\theta = 31.77^{\circ}$; 34.42°; 36.25°; 47.50°; 56.60°; 62.86°; 66.38°; 67.96°; 69.10°; and 72.86°, corresponding to the reflection from (100), (002), (101), (102), (110), (103), (200), (112), (201), and (004) planes of the standard ZnO crystal (JCPDS 36-1451). This result is consistent with the UV-Vis absorption spectra of SBA-15 and ZnO/SBA-15 (Figure 6(b)). In the UV-Vis absorption spectrum, ZnO/SBA-15 presents an amorphous and a crystalline ZnO phase shown by an absorption band in the region 240–420 nm.

Small-angle XRD patterns of the ZnO/SBA-15 and SBA-15 samples are shown in Figure 7. ZnO/SBA-15 material still has 3 peaks of (100), (110), and (200) planes of the hexagonal space group, indicating that the introduction of ZnO into SBA-15 did not collapse the mesoscopic order of a two-dimensional hexagonal structure.

TEM images of SBA-15 and ZnO/SBA-15 are shown in Figure 8. Figure 8(b) shows that the ZnO/SBA-15 material

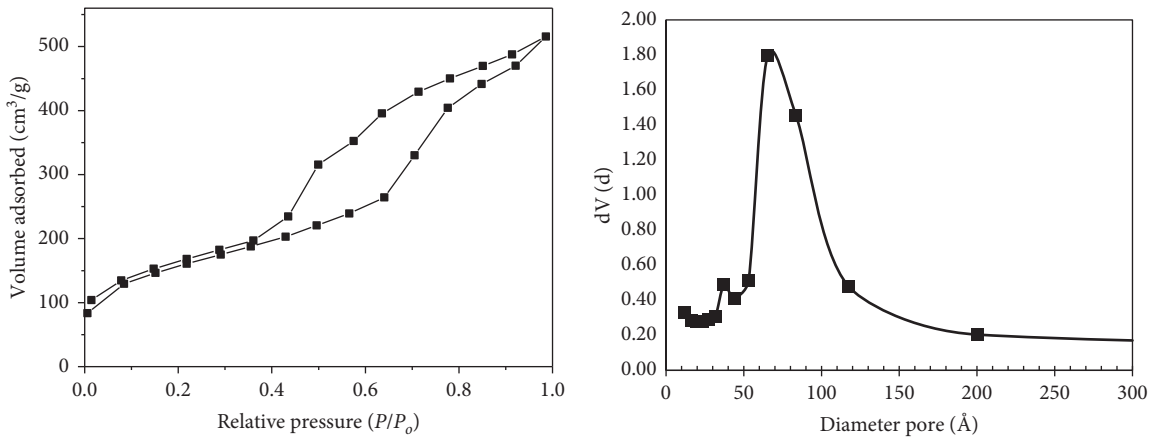

Figure 3: Adsorption-desorption isotherms of nitrogen on SBA-15 (a) and the pore size distribution of SBA-15 (b).

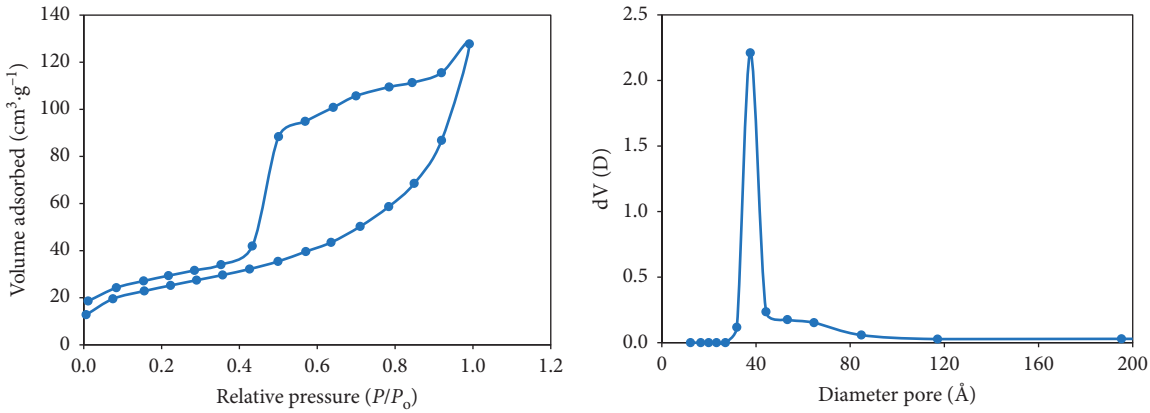

Figure 4: Adsorption-desorption isotherms of nitrogen on ZnO/SBA-15 (a); and the pore size distribution of ZnO/SBA-15 (b).

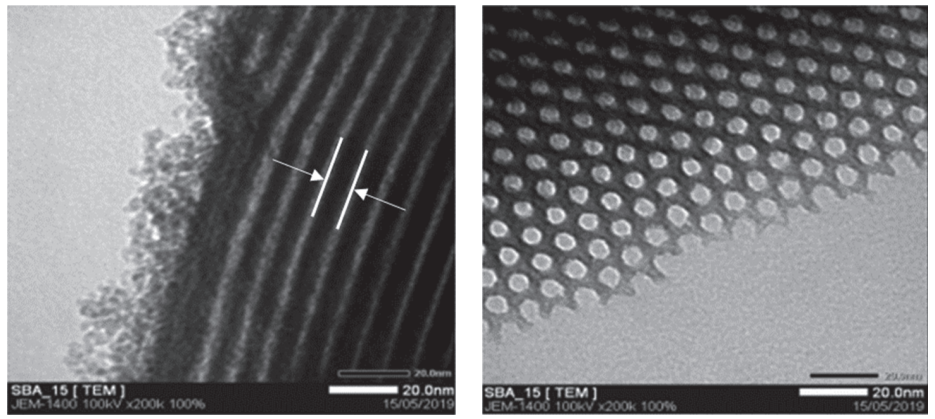

Figure 5: TEM images of SBA-15.

retains a tubular structure like SBA-15 (Figure 8(a)). Figure 8(d) shows that ZnO/SBA-15 retains the hexagonal structure of SBA-15, but the hexagonal size is reduced due to ZnO covering the inner surface of the capillary, making the capillary wall thickening and capillary tube size is reduced. The obtained results of the BET and BJH method show that the surface area, volume of pores, and pore size of ZnO/SBA-15 is 212.851 $m^2 \cdot g^{-1}$, 0.244 $cm^3 \cdot g^{-1}$, and 3.7 nm, respectively (Figure 4).

The surface of ZnO/SBA-15, SBA-15, and mass percent of elements in the materials were observed by SEM and EDS

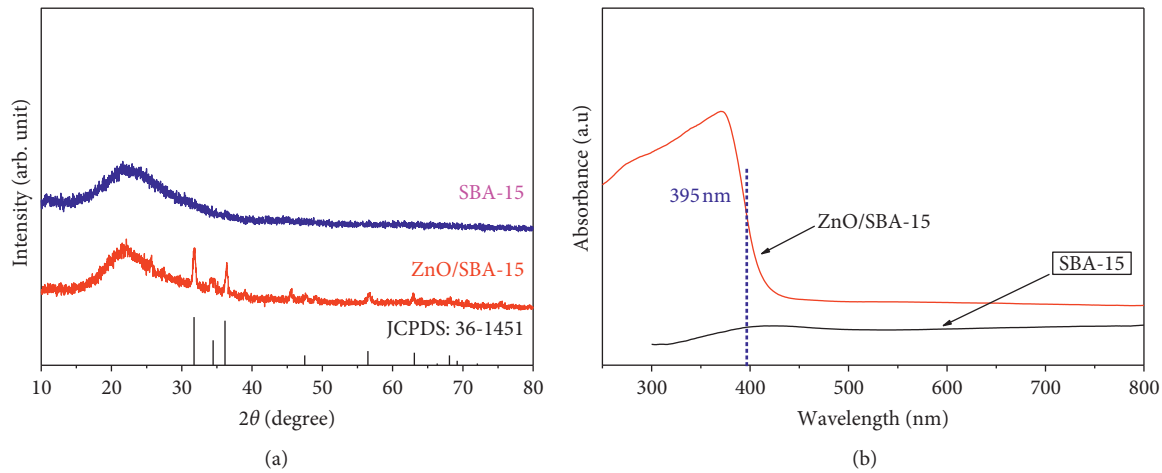

Figure 6: The high-angle XRD patterns of ZnO/SBA-15 (a) and the UV-Vis absorption spectra of SBA-15 and ZnO/SBA-15 (b).

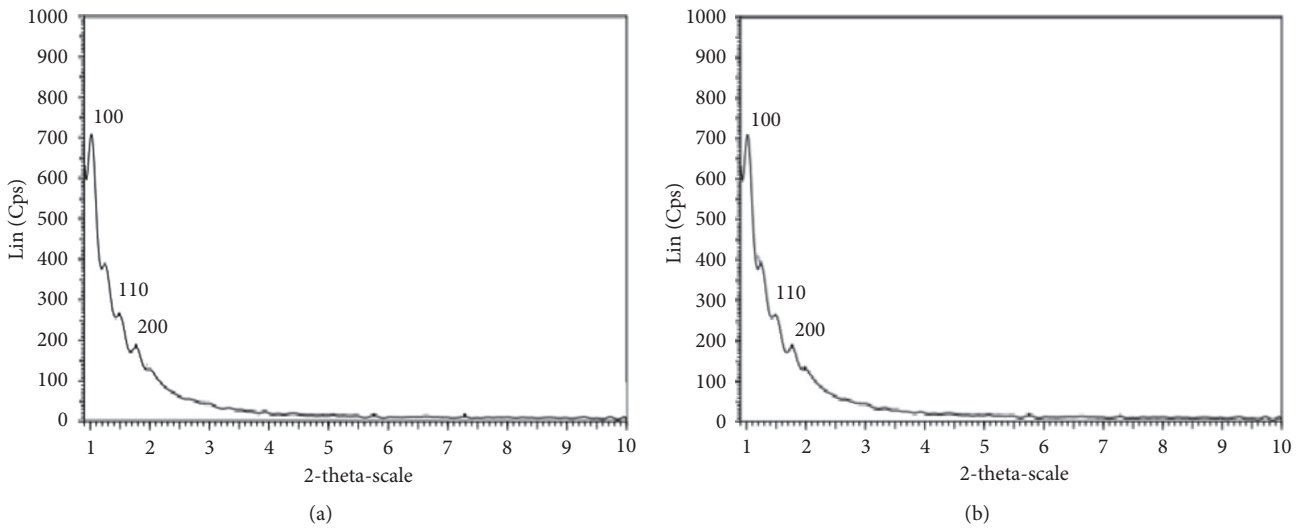

Figure 7: Small-XRD patterns of the ZnO/SBA-15 and SBA-15 samples. (a) SBA-15. (b) ZnO/SBA-15.

(Figure 9). The EDS patterns (Figures 9(a) and 9(b)) show the presence of zinc elements in the SBA structure-15. SBA-15 surface (Figure 9(c)) is the bond of large arrays, while the surface of ZnO/SBA-15 (Figure 9(d)) has the bond of smaller particles. The mass percent of elements of SBA-15 and ZnO/SBA-15 materials are listed in Table 1.

Therefore, ZnO has been successfully dispersed on the surface of SBA-15 which synthesized using the ash of brickyards without collapsing the mesoscopic order of a two-dimensional hexagonal structure.

3.3. MB Removal Capacity of Materials

3.3.1. Effect of Photocatalytic Time on MB Decomposition Capability. The optimal photocatalytic time in the MB treatment of ZnO/SBA-15 was investigated and shown in Figure 10. This investigated result shown that during the photocatalytic period from 30 to 60 min, MB concentration decreased rapidly, from 60–180 min, MB concentration fell slowly. In the period of 180–360 min, the concentration of MB is almost unchanged because the mixture was saturated. So, the optimal photocatalytic time to decompose MB (96.69% removal efficiency) is 180 mins.

3.3.2. Effect of Solid/Liquid Ratio on the Adsorption and Photocatalytic Capacity of ZnO/SBA-15. The optimal solid/liquid ratio of ZnO/SBA-15: MB was investigated and shown in Figure 11. The results showed that when the ratio of solids/liquids was adjusted in the range of 0.1–3.0, the removal efficiency of MB increased slowly (95.84%–96.75%). The efficiency was reached the highest when the ratio was 0.1 (corresponding to 5 mg ZnO/SBA-15) and decreased sharply when the solids ratio increased. The reason may be due to the light shielding effect between particles in the suspension, and this shielding is greater when the concentration of particles in the suspension is high [16]. Therefore, the solid/liquid ratio of 0.1 was chosen to use in experimental of methylene blue decomposition in solution. The maximum amounts of

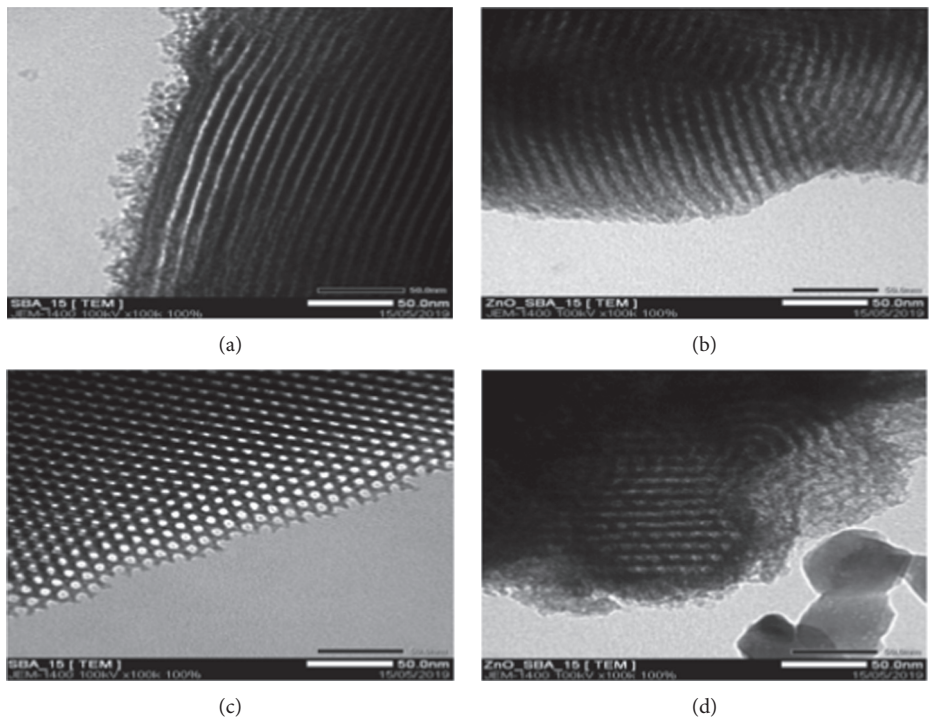

(a) (b)

(c) (d)

Figure 8: TEM images of SBA-15 (a, c) and ZnO/SBA-15 (b, d).

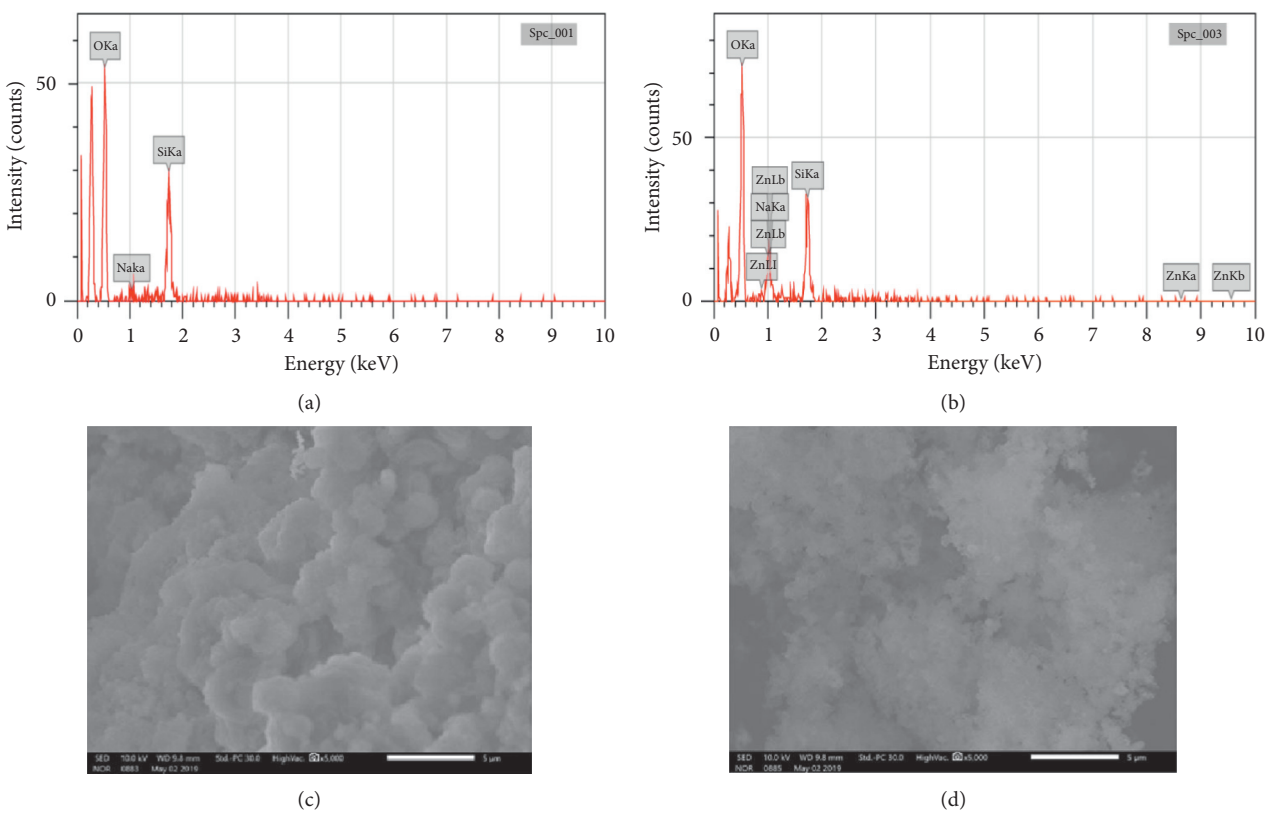

(a) (b)

(c) (d)

Figure 9: EDS spectra and SEM images of materials: (a) EDS spectrum of SBA-15; (b) EDS spectrum of ZnO/SBA-15; (c) SEM images of SBA-15; and (d) SEM images of ZnO/SBA-15.

Table 1: Mass percent of elements contained in SBA-15 and ZnO/SBA-15.

Elements	Mass percent of elements (%)	
	SBA-15	ZnO/SBA-15
O	62.72	53.05
Na	1.36	1.14
Si	35.92	26.93
Zn	0.00	19.89

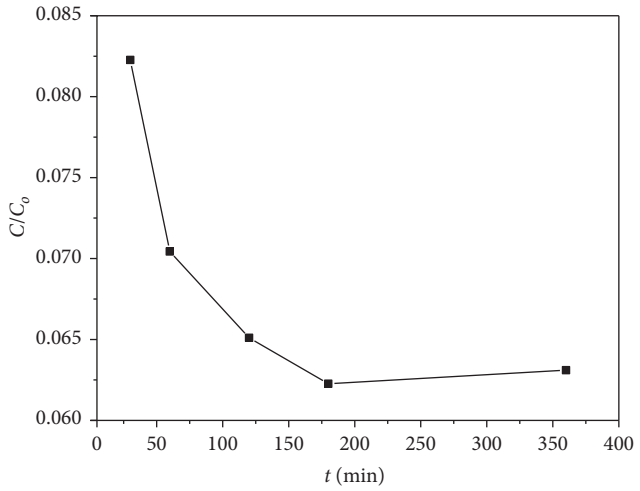

Figure 10: The change in the relative concentration of MB in solution with UV light irradiation time.

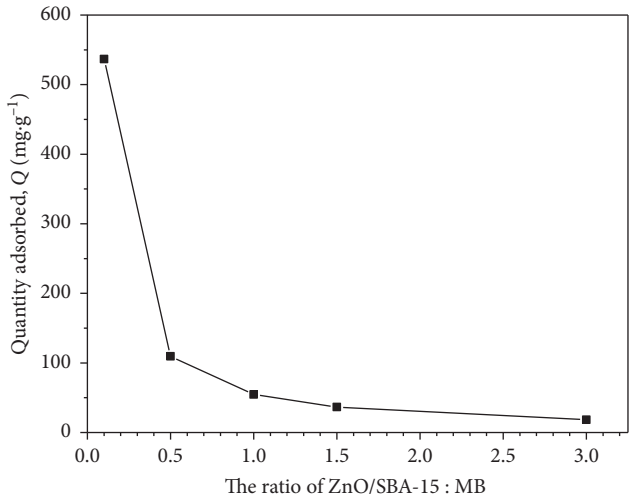

Figure 11: Effect of the ratio of ZnO/SBA-15: MB on photocatalytic capacity of ZnO/SBA-15 materials.

MB adsorbed (Q, mg·g^{-1}) by ZnO/SBA-15 along with other adsorbents is shown in Table 2. In comparison with other adsorbents, ZnO/SBA-15 is promising material for removal of the MB from aqueous solutions.

3.3.3. Efficient Catalyst Reuse. After each decomposition experiment, the ZnO/SBA-15 catalyst was recovered by filtration, washing with water, and dried for reuse. The efficient catalyst reuse of ZnO/SBA-15 material after reusing 5 times are shown in Figure 12. The investigated result indicates that the MB removal efficiencies of ZnO/SBA-15 after reusing 5 times were reached more 94%.

Table 2: The comparison of the maximum adsorption capacity of MB on ZnO/SBA-15 material with other adsorbents.

Adsorbents	Q (mg·g^{-1})	Reference
Mn/MCM-41	131.6	[17]
Porous silicon-carbon-nitrogen hybrid materials	291.8	[18]
ZnO/congo red	43.5	[19]
Zn-doped SiO_2/TiO_2	20.0	[20]
ZnO/SBA-15	536.7	This work

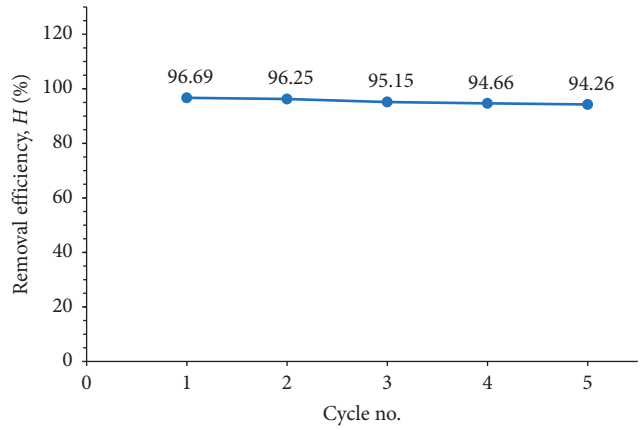

Figure 12: MB removal efficiencies of ZnO/SBA-15 catalyst after reusing 5 times.

4. Conclusions

SBA-15 mesoporous material was successfully prepared by using the ash of brickyards. The SBA-15 material has the surface area of 700.100 m^2·g^{-1}, pore volume of 0.813 cm^3·g^{-1}, and pore size of 7.5 nm. These results were determined by the analysis methods as FTIR, XRD, TEM, EDS and BET, BJH.

The results of the structural characteristic methods (FTIR, UV-Vis, XRD, SEM, TEM, EDS, BET, and BJH) shown that the material ZnO/SBA-15 was successfully synthesized. The mesoporous channels of SBA-15 is also retained in ZnO/SBA-15 with surface area, pore volume, and pore size, respectively: 212.851 m^2·g^{-1}, 0.244 cm^3·g^{-1}, and 3.7 nm.

The methylene blue removal capacity of ZnO/SBA-15 was generally investigated. The MB removal efficiency of ZnO/SBA-15 was reached 96.69% with initial concentration of MB of 56 ppm; the photocatalytic time of 180 mins and the optimal solid/liquid ratio of 0.1. Especially, the MB removal efficiencies of ZnO/SBA-15 after reusing 5 times were reached more 94%.

Data Availability

The data used to support the findings of this study are included within the article.

Conflicts of Interest

The authors declare that they have no conflicts of interest.

Acknowledgments

The authors wish to thank Saigon University, Ho Chi Minh, Vietnam, for their financial support of this work.

References

[1] D. Zhao, J. L. Feng, Q. S. Huo et al., "Triblock copolymer syntheses of mesoporous silica with periodic 50 to 300; angstrom pores," *Science*, vol. 279, no. 5350, pp. 548–552, 1998.

[2] V.-T. Hoang, Q. Huang, M. Eić, T.-O. Do, and S. Kaliaguine, "Structure and diffusion characterization of SBA-15 materials," *Langmuir*, vol. 21, no. 5, pp. 2051–2057, 2005.

[3] Y.-J. Han, G. D. Stucky, and A. Butler, "Mesoporous silicate sequestration and release of proteins," *Journal of the American Chemical Society*, vol. 121, no. 42, pp. 9897-9898, 1999.

[4] C. Hess, "Nanostructured vanadium oxide model catalysts for selective oxidation reactions," *ChemPhysChem*, vol. 10, no. 2, pp. 319–326, 2009.

[5] M. Cavalleri, K. Hermann, A. Knop-Gericke et al., "Analysis of silica-supported vanadia by X-ray absorption spectroscopy: combined theoretical and experimental studies," *Journal of Catalysis*, vol. 262, no. 2, pp. 215–223, 2009.

[6] R. Ryoo, C. H. Ko, M. Kruk, V. Antochshuk, and M. Jaroniec, "Block-copolymer-templated ordered mesoporous silica: array of uniform mesopores or mesopore–micropore network?" *The Journal of Physical Chemistry B*, vol. 104, no. 48, pp. 11465–11471, 2000.

[7] C. Yu, J. Fan, B. Tian, and D. Zhao, "Morphology development of mesoporous materials: a colloidal phase separation mechanism," *Chemistry of Materials*, vol. 16, no. 5, pp. 889–898, 2004.

[8] N. Rahmat, F. Hamzah, N. Sahiron, M. Mazlan, and M. M. Zahari, "Sodium silicate as source of silica for synthesis of mesoporous SBA-15," *IOP Conference Series: Materials Science and Engineering*, vol. 133, Article ID 012011, 2016.

[9] J. Puputti, H. Jin, J. Rosenholm, H. Jiang, and M. Lindén, "The use of an impure inorganic precursor for the synthesis of highly siliceous mesoporous materials under acidic conditions," *Microporous and Mesoporous Materials*, vol. 126, no. 3, pp. 272–275, 2009.

[10] P. Dai, T.-T. Yan, X.-X. Yu, Z.-M. Bai, and M.-Z. Wu, "Two-solvent method synthesis of NiO/ZnO nanoparticles embedded in mesoporous SBA-15: photocatalytic properties study," *Nanoscale Research Letters*, vol. 11, no. 1, p. 226, 2016.

[11] G. D. Mihai, V. Meynen, M. Mertens, N. Bilba, P. Cool, and E. F. Vansant, "ZnO nanoparticles supported on mesoporous MCM-41 and SBA-15: a comparative physicochemical and photocatalytic study," *Journal of Materials Science*, vol. 45, no. 21, pp. 5786–5794, 2010.

[12] M. D. Driessen, T. M. Miller, and V. H. Grassian, "Photocatalytic oxidation of trichloroethylene on zinc oxide: characterization of surface-bound and gas-phase products and intermediates with FT-IR spectroscopy," *Journal of Molecular Catalysis A: Chemical*, vol. 131, no. 1–3, pp. 149–156, 1998.

[13] R. Ullah and J. Dutta, "Photocatalytic degradation of organic dyes with manganese-doped ZnO nanoparticles," *Journal of Hazardous Materials*, vol. 156, no. 1–3, pp. 194–200, 2008.

[14] K. Byrappa, A. S. Dayananda, C. P. Sajan et al., "Hydrothermal preparation of ZnO:CNT and TiO2:CNT composites and their photocatalytic applications," *Journal of Materials Science*, vol. 43, no. 7, pp. 2348–2355, 2008.

[15] J. Berthelin, P. M. Huang, J.-M. Bollag, and F. Andreux, *Adsorption of Methylene Blue by Red Mud, an Oxide- Rich Byproduct of Bauxite Refining*, Springer, Berlin, Germany, 1999.

[16] O. Carp, C. L. Huisman, and A. Reller, "Photoinduced reactivity of titanium dioxide," *Progress in Solid State Chemistry*, vol. 32, no. 1-2, pp. 33–177, 2004.

[17] M. M. Ayad and A. A. El-Nasr, "Adsorption of cationic dye (methylene blue) from water using polyaniline nanotubes base," *The Journal of Physical Chemistry C*, vol. 114, no. 34, pp. 14377–14383, 2010.

[18] L. Meng, X. Zhang, Y. Tang, K. Su, and J. Kong, "Hierarchically porous silicon-carbon-nitrogen hybrid materials towards highly efficient and selective adsorption of organic dyes," *Scientific Reports*, vol. 5, no. 1, p. 7910, 2015.

[19] T. M. Elmorsi, M. H. Elsayed, and M. F. Bakr, "Enhancing the removal of methylene blue by modified ZnO nanoparticles: kinetics and equilibrium studies," *Canadian Journal of Chemistry*, vol. 95, no. 5, pp. 590–600, 2017.

[20] S. Ahmad and A. Saeed, "Synthesis of metal/silica/titania composites for the photocatalytic removal of methylene blue dye," *Journal of Chemistry*, vol. 2019, pp. 1–6, 2019.